ELECTRONICS

Electronic plants

10.1126/sciadv.1501136

Eleni Stavrinidou,[1] Roger Gabrielsson,[1]* Eliot Gomez,[1]* Xavier Crispin,[1] Ove Nilsson,[2] Daniel T. Simon,[1] Magnus Berggren[1]†

The roots, stems, leaves, and vascular circuitry of higher plants are responsible for conveying the chemical signals that regulate growth and functions. From a certain perspective, these features are analogous to the contacts, interconnections, devices, and wires of discrete and integrated electronic circuits. Although many attempts have been made to augment plant function with electroactive materials, plants' "circuitry" has never been directly merged with electronics. We report analog and digital organic electronic circuits and devices manufactured in living plants. The four key components of a circuit have been achieved using the xylem, leaves, veins, and signals of the plant as the template and integral part of the circuit elements and functions. With integrated and distributed electronics in plants, one can envisage a range of applications including precision recording and regulation of physiology, energy harvesting from photosynthesis, and alternatives to genetic modification for plant optimization.

INTRODUCTION

The growth and function of plants are powered by photosynthesis and are orchestrated by hormones and nutrients that are further affected by environmental, physical, and chemical stimuli. These signals are transported over long distances through the xylem and phloem vascular circuits to selectively trigger, modulate, and power processes throughout the organism (*1*) (see Fig. 1). Rather than tapping into this vascular circuitry, artificial regulation of plant processes is achieved today by exposing the plant to exogenously added chemicals or through molecular genetic tools that are used to endogenously change metabolism and signal transduction pathways in more or less refined ways (*2*). However, many long-standing questions in plant biology are left unanswered because of a lack of technology that can precisely regulate plant functions locally and in vivo. There is thus a need to record, address, and locally regulate isolated—or connected—plant functions (even at the single-cell level) in a highly complex and spatiotemporally resolved manner. Furthermore, many new opportunities will arise from technology that harvests or regulates chemicals and energy within plants. Specifically, an electronic technology leveraging the plant's native vascular circuitry promises new pathways to harvesting from photosynthesis and other complex biochemical processes.

Organic electronic materials are based on molecules and polymers that conduct and process both electronic (electrons e^-, holes h^+) and ionic (cations A^+, anions B^-) signals in a tightly coupled fashion (*3*, *4*). On the basis of this coupling, one can build up circuits of organic electronic and electrochemical devices that convert electronic addressing signals into highly specific and complex delivery of chemicals (*5*), and vice versa (*6*), to regulate and sense various functions and processes in biology. Such "organic bioelectronic" technology platforms are currently being explored in various medical and sensor settings, such as drug delivery, regenerative medicine, neuronal interconnects, and diagnostics. Organic electronic materials—amorphous or ordered electronic and iontronic polymers and molecules—can be manufactured into device systems that exhibit a unique combination of properties and can be shaped into almost any form using soft and even living systems (*7*) as the template (*8*). The electronically conducting polymer poly(3,4-ethylenedioxythiophene) (PEDOT) (*9*), either doped with polystyrene sulfonate (PEDOT:PSS) or self-doped (*10*) via a covalently attached anionic side group [for example, PEDOT-S:H (*8*)], is one of the most studied and explored organic electronic materials (see Fig. 1E). The various PEDOT material systems typically exhibit high combined electronic and ionic conductivity in the hydrated state (*11*). PEDOT's electronic performance and characteristics are tightly coupled to charge doping, where the electronically conducting and highly charged regions of $PEDOT^+$ require compensation by anions, and the neutral regions of $PEDOT^0$ are uncompensated. This "electrochemical" activity has been extensively utilized as the principle of operation in various organic electrochemical transistors (OECTs) (*12*), sensors (*13*), electrodes (*14*), supercapacitors (*15*), energy conversion devices (*16*), and electrochromic display (OECD) cells (*9*, *17*). PEDOT-based devices have furthermore excelled in regard to compatibility, stability, and bioelectronic functionality when interfaced with cells, tissues, and organs, especially as the translator between electronic and ionic (for example, neurotransmitter) signals. PEDOT is also versatile from a circuit fabrication point of view, because contacts, interconnects, wires, and devices, all based on PEDOT:PSS, have been integrated into both digital and analog circuits, exemplified by OECT-based logical NOR gates (*18*) and OECT-driven large-area matrix-addressed OECD displays (*17*) (see Fig. 1B).

In the past, artificial electroactive materials have been introduced and dispensed into living plants. For instance, metal nanoparticles (*19*), nanotubes (*20*), and quantum dots (*21*) have been applied to plant cells and the vascular systems (*22*) of seedlings and/or mature plants to affect various properties and functions related to growth, photosynthesis, and antifungal efficacy (*23*). However, the complex internal structure of plants has never been used as a template for in situ fabrication of electronic circuits. Given the versatility of organic electronic materials—in terms of both fabrication and function—we investigated introducing electronic functionality into plants by means of PEDOT.

RESULTS AND DISCUSSION

We chose to use cuttings of *Rosa floribunda* (garden rose) as our model plant system. The lower part of a rose stem was cut, and the fresh cross section was immersed in an aqueous PEDOT-S:H solution for 24 to 48 hours (Fig. 2A), during which time the PEDOT-S:H solution was

[1]Laboratory of Organic Electronics, Department of Science and Technology, Linköping University, SE-601 74 Norrköping, Sweden. [2]Department of Forest Genetics and Plant Physiology, Swedish University of Agricultural Sciences, SE-901 87 Umeå, Sweden.
*These authors contributed equally to this work.
†Corresponding author. E-mail: magnus.berggren@liu.se

taken up into the xylem vascular channel and transported apically. The rose was taken from the solution and rinsed in water. The outer bark, cortex, and phloem of the bottom part of the stem were then gently peeled off, exposing dark continuous lines along individual 20- to 100-μm-wide xylem channels (Fig. 2). In some cases, these "wires" extended >5 cm along the stem. From optical and scanning electron microscopy images of fresh and freeze-dried stems, we conclude that the PEDOT-S:H formed sufficiently homogeneously ordered hydrogel wires occupying the xylem tubular channel over a long range. PEDOT-S:H is known to form hydrogels in aqueous-rich environments, in particular in the presence of divalent cations, and we assume that this is also the case for the wires established along the xylem channels of rose stems. The conductivity of PEDOT-S:H wires was measured using two Au probes applied into individual PEDOT-S:H xylem wires along the stem (Fig. 3A). From the linear fit of resistance versus distance between the contacts, we found electronic conductivity to be 0.13 S/cm with contact resistance being ~10 kilohm (Fig. 3B). To form a hydrogel-like and continuous wire along the inner surface and volume of a tubular structure, such as a xylem channel, by exposing only its tiny inlet to a solution, we must rely on a subtle thermodynamic balance of transport and kinetics. The favorability of generating the initial monolayer along the inner wall of the xylem, along with the subsequent reduction in free energy of PEDOT-S:H upon formation of a continuous hydrogel, must be in proper balance with respect to the unidirectional flow, entropy, and diffusion properties of the solution in the xylem. Initially, we explored an array of different conducting polymer systems to generate wires along the rose stems (table S1). We observed either clogging of the materials already at the inlet or no adsorption of the conducting material along the xylem whatsoever. On the basis of these cases, we conclude that the balance between transport, thermodynamics, and kinetics does not favor the formation of wires inside xylem vessels. In addition, we attempted in situ chemical or electrochemical polymerization of various monomers [for example, pyrrole, aniline, EDOT (3,4-ethylenedioxythiophene), and derivatives] inside the plant. For chemical polymerization, we administered the monomer solution to the plant, followed by the oxidant solution. Although some wire fragments were formed, the oxidant solution had a strong toxic effect. For electrochemical polymerization, we observed successful formation of conductors only in

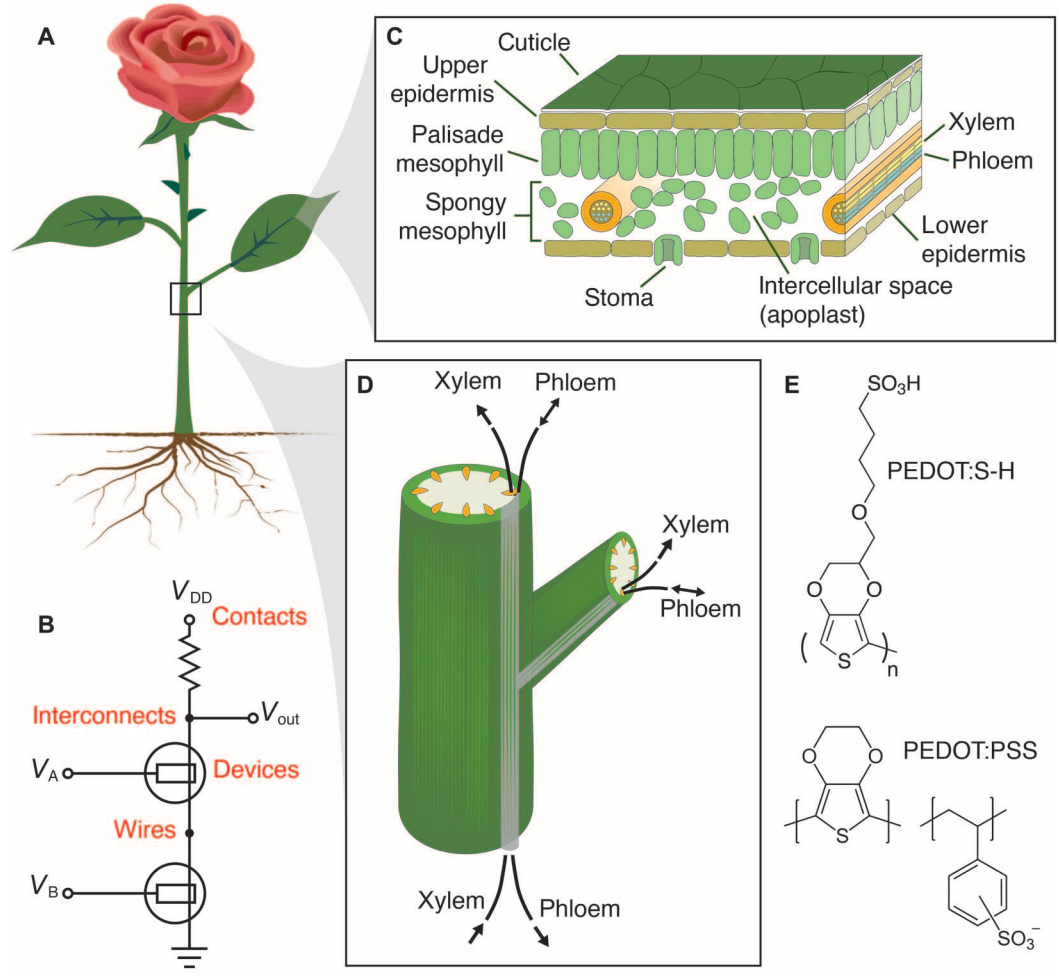

Fig. 1. Basic plant physiology and analogy to electronics. (**A** and **B**) A plant (A), such as a rose, consists of roots, branches, leaves, and flowers similar to (B) electrical circuits with contacts, interconnects, wires, and devices. (**C**) Cross section of the rose leaf. (**D**) Vascular system of the rose stem. (**E**) Chemical structures of PEDOT derivatives used.

proximity to the electrode. PEDOT-S:H was the only candidate that formed extended continuous wires along the xylem channels.

It is known that the composition of cations is regulated within the xylem; that is, monovalent cations are expelled from the xylem and exchanged with divalent cations (*24*). After immersing the rose stem into the aqueous solution, dissolved PEDOT-S:H chains migrated along the xylem channels, primarily driven by the upward cohesion-tension transportation of water. We hypothesize that a net influx of divalent cations into the xylem occurred, which then increased the chemical kinetics for PEDOT-S:H to form a homogeneous and long-range hydrogel conductor phase along the xylem circuitry. The surprisingly high conductivity (>0.1 S/cm) of these extended PEDOT-S:H wires suggests that swift transport and distribution of dissolved PEDOT-S:H chains along the xylem preceded the formation of the actual conductive hydrogel wires.

These long-range conducting PEDOT-S:H xylem wires, surrounded with cellular domains including confined electrolytic compartments, are promising components for developing in situ OECT devices and other electrochemical devices and circuits. We therefore proceeded to investigate transistor functionality in the xylem wires. A single PEDOT-S:H xylem wire simultaneously served as the transistor channel, source, and drain of an OECT. The gate comprised a PEDOT:PSS–coated Au probe coupled electrolytically through the plant cells and extracellular medium surrounding the xylem (Fig. 4A, inset). Two additional Au probes defined the source and the drain contacts. By applying a positive potential to the gate electrode (V_G) with respect to the grounded source, the number of charge carriers (h^+) in the OECT channel is depleted, via ion exchange (A^+) with the extracellular medium and charge compensation at the gate electrode. This mechanism defines the principle of operation of the xylem-OECT. The device exhibited the expected output characteristics of an OECT (Fig. 4A). Electronic drain current (I_D) saturation is also seen, which is caused by pinch-off within the channel near the drain electrode. Figure 4B shows the transfer curve, and Fig. 4C shows the temporal evolution of I_D and the gate current (I_G) with increasing V_G. From these measurements, we calculate an I_D on/off ratio of ~40, a transconductance ($\Delta I_D/\Delta V_G$) reaching 14 μS at V_G = 0.3 V, and very little current leakage from the gate into the channel and drain ($\partial I_D/\partial I_G$ > 100 at V_G = 0.1 V).

With OECTs demonstrated, we proceeded to investigate more complex xylem-templated circuits, namely, xylem logic. Two xylem-OECTs were formed in series by applying two PEDOT:PSS–coated Au gate probes at different positions along the same PEDOT-S:H xylem

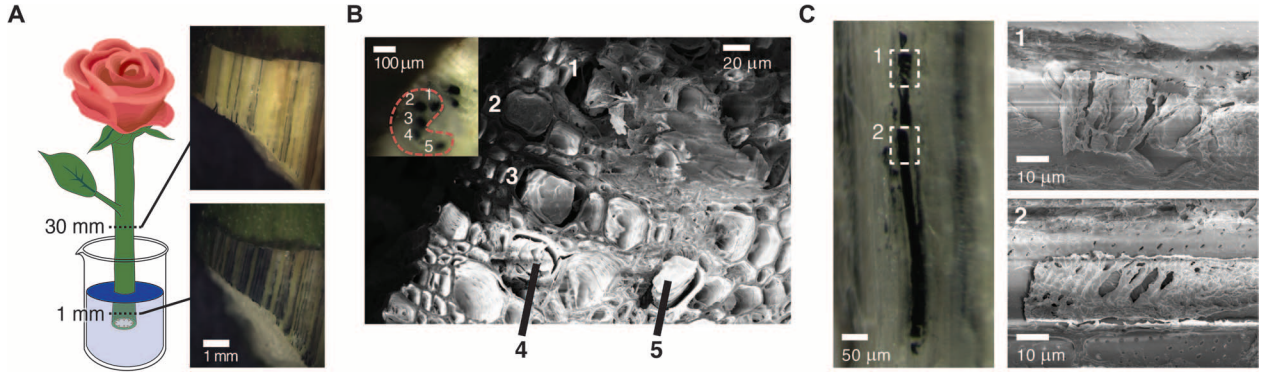

Fig. 2. Electronically conducting xylem wires. (**A**) Forming PEDOT-S:H wires in the xylem. A cut rose is immersed in PEDOT-S:H aqueous solution, and PEDOT-S:H is taken up and self-organizes along the xylem forming conducting wires. The optical micrographs show the wires 1 and 30 mm above the bottom of the stem (bark and phloem were peeled off to reveal the xylem). (**B**) Scanning electron microscopy (SEM) image of the cross section of a freeze-dried rose stem showing the xylem (1 to 5) filled with PEDOT-S:H. The inset shows the corresponding optical micrograph, where the filled xylem has the distinctive dark blue color of PEDOT. (**C**) SEM images (with corresponding micrograph on the left) of the xylem of a freeze-dried stem, which shows a hydrogel-like PEDOT-S structure.

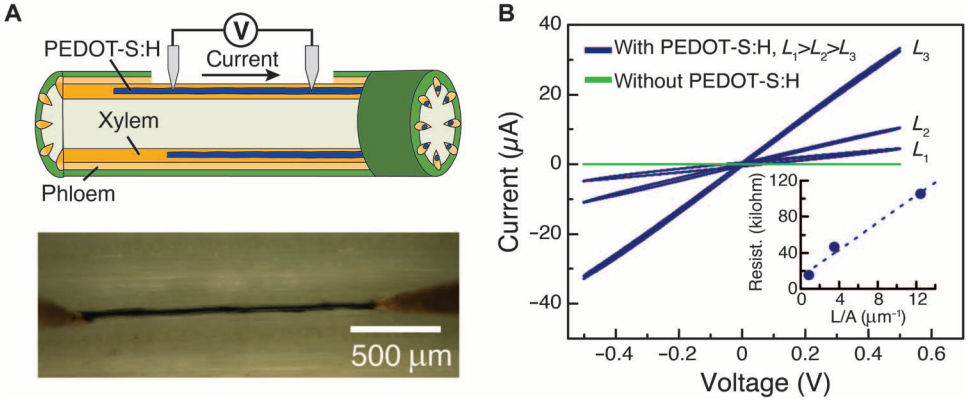

Fig. 3. Electrical characterization of xylem wires. (**A**) Schematic of conductivity measurement using Au probes as contacts. (**B**) *I-V* characteristics of PEDOT-S xylem wires of different lengths: L_1 = 2.15 mm, L_2 = 0.9 mm, and L_3 = 0.17 mm. The inset shows resistance versus length/area and linear fit, yielding a conductivity of 0.13 S/cm.

wire. The two OECTs were then connected, via two Au probes, to an external 800-kilohm resistor connected to a supply voltage (V_{DD} = −1.5 V) on one side and to an electric ground on the other side (Fig. 4D). The two gate electrodes defined separate input terminals, whereas the output terminal coincides with the drain contact of the "top" OECT (that is, the potential between the external resistor and the OECT). By applying different combinations of input signals (0 V as digital "0" or +0.5 V as "1"), we observed NOR logic at the output, in the form of voltage below −0.5 V as "0" and that above −0.3 V as "1."

In addition to xylem and phloem vascular circuitry, leaves comprise the palisade and spongy mesophyll, sandwiched between thin upper and lower epidermal layers (Fig. 1C). The spongy mesophyll, distributed along the abaxial side of the leaf, contains photosynthetically active cells surrounded by the apoplast: the heavily hydrated space between cell walls essential to several metabolic processes, such as sucrose transport and gas exchange. Finally, the stomata and their parenchymal guard cells gate the connection between the surrounding air and the spongy mesophyll and apoplast, and regulate the important O_2-CO_2 exchange. Together, these structures and functions of the abaxial side of the leaf encouraged us to explore the possibility of establishing areal—and potentially segmented—electrodes in leaves in vivo.

Vacuum infiltration (*25*, *26*) is a technique commonly used in plant biology to study metabolite (*27*) and ion concentrations in the apoplastic fluid of leaves. We used this technique to "deposit" PEDOT:PSS, combined with nanofibrillar cellulose (PEDOT:PSS–NFC), into the apoplast of rose leaves. PEDOT:PSS–NFC is a conformable, self-supporting, and self-organized electrode system that combines high electronic and ionic conductivity (*28*). A rose leaf was submerged in a syringe containing an aqueous PEDOT:PSS–NFC solution. The syringe was plunged to remove air and sealed at the nozzle, and the plunger was then gently pulled to create vacuum (Fig. 5A), thus forcing air out of the leaf through the stomata. As the syringe returned to its original position, PEDOT:PSS–NFC was drawn in through the stomata to reside in the spongy mesophyll (Fig. 5B). A photograph of a pristine leaf and the microscopy of its cross section (Fig. 5, C and D) are compared to a leaf infiltrated with PEDOT:PSS–NFC (Fig. 5, E and F). PEDOT:PSS–NFC appeared to be confined in compartments, along the abaxial side of the leaf, delineated by the vascular network in the mesophyll (Fig. 5F). The result was a leaf composed of a two-dimensional (2D) network of compartments filled—or at least partially filled—with the electronic-ionic PEDOT:PSS–NFC electrode material. Some compartments appeared darker and some did not change color at all, suggesting that the amount of PEDOT:PSS–NFC differed between compartments.

We proceeded to investigate the electrochemical properties of this 2D circuit network using freestanding PEDOT:PSS–NFC films (area, 1 to 2 mm^2; thickness, 90 μm; conductivity, ~19 S/cm; ionic charge capacity, ~0.1 F) placed on the outside of the leaf, providing electrical contacts through the stomata to the material inside the leaf. We observed typical charging-discharging characteristics of a two-electrode electrochemical cell while observing clear electrochromism compartmentalized by the mesophyll vasculature (Fig. 6, A and B, and movie S1). Upon applying a constant bias, steady-state electrochromic switching of all active

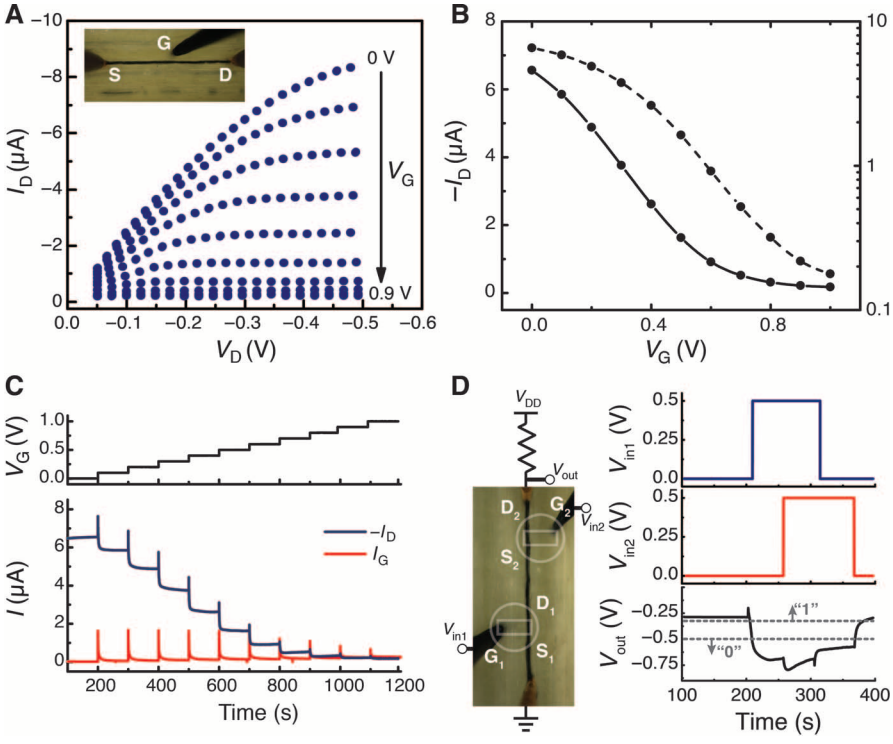

Fig. 4. Xylem transistors and digital logic. (**A**) Output characteristics of the xylem-OECT. The inset shows the xylem wire as source (S) and drain (D) with gate (G) contacted through the plant tissue. (**B**) Transfer curve of a typical xylem-OECT for V_D = −0.3 V (solid line, linear axis; dashed line, log axis). (**C**) Temporal response of I_D and I_G relative to increasing V_G. (**D**) Logical NOR gate constructed along a single xylem wire. The circuit diagram indicates the location of the two xylem-OECTs and external connections (compare with circuit in Fig. 1B). Voltage traces for V_{in1}, V_{in2}, and V_{out} illustrate NOR function. The dashed lines on the V_{out} plot indicate thresholds for defining logical 0 and 1.

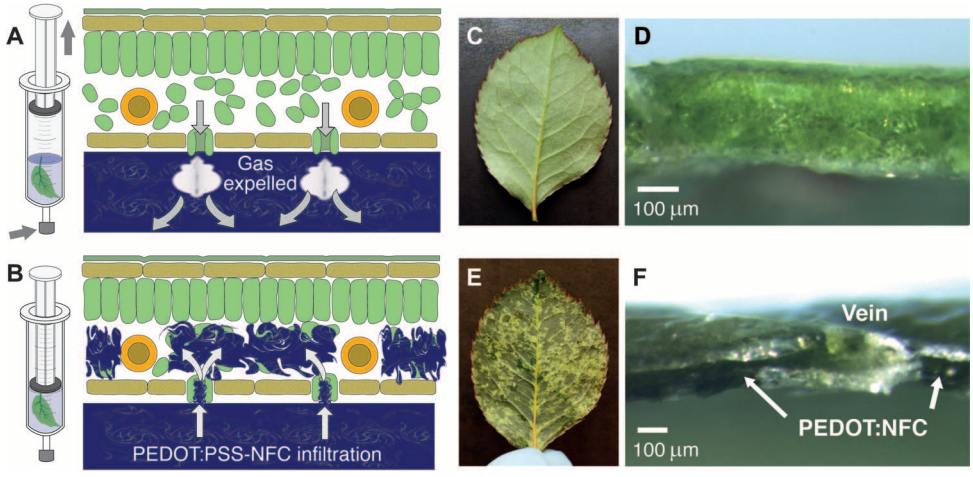

Fig. 5. PEDOT-infused leaves. (**A**) Vacuum infiltration. Leaf placed in PEDOT:PSS–NFC solution in a syringe with air removed. The syringe is pulled up, creating negative pressure and causing the gas inside the spongy mesophyll to be expelled. (**B**) When the syringe returns to standard pressure, PEDOT:PSS–NFC is infused through the stomata, filling the spongy mesophyll between the veins. (**C** and **D**) Photograph of the bottom (C) and cross section (D) of a pristine rose leaf before infiltration. (**E** and **F**) Photograph of the bottom (E) and cross section (F) of leaf after PEDOT:PSS–NFC infusion.

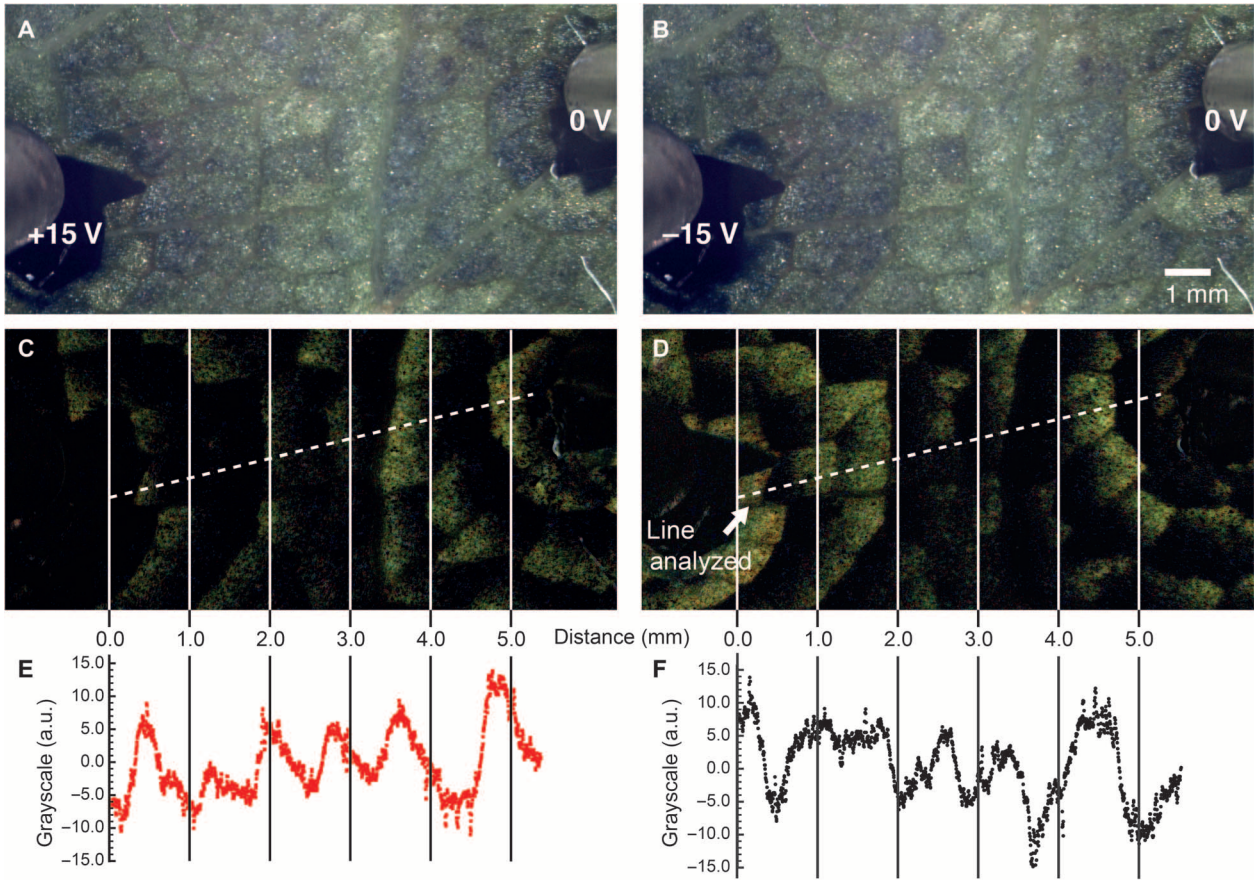

Fig. 6. Electrochromism in PEDOT:PSS–NFC–infused leaf. (**A** and **B**) Optical micrographs of the infused leaf upon application of (A) +15 V and (B) −15 V. Movie S1 shows a video recording of these results. (**C** and **D**) False color map of change in grayscale intensity between application of (C) +15 V and (D) −15 V. Green represents a positive increase in grayscale value (light to dark). (**E** and **F**) Grayscale values of pixel intensity along the lines indicated in (C) and (D) showing successive oxidation/reduction gradients. A plot of the change in grayscale intensity over a fixed line showing the change and oxidation/reduction gradations versus distance. a.u., arbitrary unit.

compartments typically took less than 20 s, and the effect could be maintained over an extended period of time (>10 min). Likewise, when the voltage was reversed, the observed light-dark pattern was flipped within 20 s. The electrochromism can be quantified by mapping the difference in grayscale intensity between the two voltage states (Fig. 6, C to F). The analysis shows homogeneous electrochromism in the compartments in direct stomatal contact with the external PEDOT:PSS–NFC electrodes. This is to be expected, because stomatal contact provides both ionic and electronic pathways to the external electrodes, allowing continuous electronic charging/discharging of the PEDOT and subsequent ionic compensation. However, for the intermediate compartments not in direct stomatal contact with the external electrodes, we observed electrochromic gradients with the dark-colored side ($PEDOT^0$) pointing toward the positively biased electrode. This behavior can be explained by a lack of electronic contact between these compartments—that is, the infiltrated PEDOT:PSS–NFC did not cross between compartments. As such, these intermediate compartments operate as bipolar electrodes (*29*), exhibiting so-called induced electrochromism (*30*). Indeed, the direction of the electrochromic gradients, reflecting the electric potential gradients inside the electrolyte of each compartment, exactly matches the expected pattern of induced electrochromism (Fig. 7A).

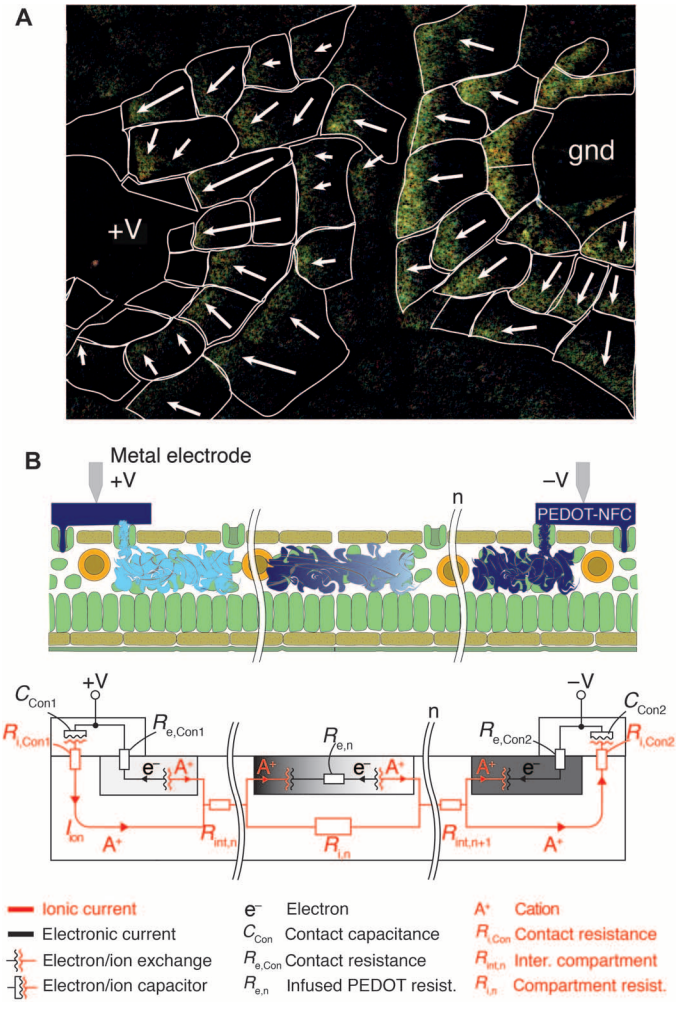

Fig. 7. Leaf OECD. (**A**) Visualization of the electric field in the leaf-OECD via the induced electrochromic gradient directions [cf. study by Said *et al.* (*30*)]. (**B**) Electrical schematic representation of n-compartments modeling both electronic and ionic components of the current.

In Fig. 7B, we propose a circuit diagram to describe the impedance characteristics and current pathways of the leaf-OECD, taking into account both the electronic and ionic current pathways. The fact that both electrochromic and potential gradients are established in electronically isolated but ionically connected areal compartments ($R_{int,n}$) along the leaf suggests that the ionic ($R_{i,Con}$) and electronic ($R_{e,Con}$) contact resistances across the stomata do not limit the charge transfer and transport. Although electrochromic switching takes less than 20 s, a constant current (due to charge compensation and ion exchange) can be maintained for extended periods of time, suggesting that the capacitance for ion compensation within the electrodes (C_{Con}) is very large, thus not limiting the current and transient behavior either. We also found that the induced electrochromism vanished shortly after the two outer electrodes were grounded, suggesting that the electronic resistance ($R_{e,n}$) of the infused PEDOT:PSS–NFC is lower than that of the parallel ionic resistance ($R_{i,n}$). Our conclusion is that the switch rate of directly and indirectly induced compartments of the leaf-OECD is limited by ionic—rather than electronic—transport.

The fact that electrochromically visualized potential gradients are established along leaf compartments indicates that ion conduction across veins is efficient and does not limit the overall charge transport. Indeed, we demonstrate above that induced electrochromism and optical image analysis are powerful tools to investigate ion migration pathways within a leaf. However, many technological opportunities and tools require extended electronic conduction along the entire leaf. Our next target will therefore include development of conductive bridges that can transport electronic charges across leaf veins as well.

All experiments on OECT and OECD circuits, in the xylem and in leaves, were carried out on plant systems where the roots or leaves had been detached from the plant. In a final experiment, we investigated infusion of PEDOT:PSS–NFC into a single leaf still attached to a living rose, with maintained root, stem, branches, and leaves. We found infusion of PEDOT:PSS–NFC to be successful and we observed OECD switching similar to the isolated leaf experiments (Supplementary Materials and fig. S1).

CONCLUSIONS

Ionic transport and conductivity are fundamental to plant physiology. However, here we demonstrate the first example of electronic functionality added to plants and report integrated organic electronic analog and digital circuits manufactured in vivo. The vascular circuitry, components, and signals of *R. floribunda* plants have been intermixed with those of PEDOT structures. For xylem wires, we show long-range electronic (hole) conductivity on the order of 0.1 S/cm, transistor modulation, and digital logic function. In the leaf, we observe field-induced electrochromic gradients suggesting higher hole conductivity in isolated compartments but higher ionic conductivity across the whole leaf. Our findings pave the way for new technologies and tools based on the amalgamation of organic electronics and plants in general. For future electronic plant technologies, we identify integrated and distributed delivery and sensor devices as a particularly interesting e-Plant concept for feedback-regulated control of plant physiology, possibly serving as a complement to existing molecular genetic techniques used in plant science and agriculture. Distributed conducting wires and electrodes along the stems and roots and in the leaves are preludes to electrochemical fuel

cells, charge transport, and storage systems that convert sugar produced from photosynthesis into electricity, in vivo.

MATERIALS AND METHODS

PEDOT-S wire formation in rose xylem

We used stems directly cut from a young "Pink Cloud" *R. floribunda*, with and without flowers, purchased from a local flower shop. The stems were kept in water and under refrigeration until they were used for the experiment. The stems were cleaned with tap water and then a fresh cut was made to the bottom of the stem with a sterilized scalpel under deionized (DI) water. The stem was then immersed in PEDOT-S:H (1 mg/ml) in DI water and kept at about 40% humidity and 23°C. Experiments were performed at 70% humidity as well, but no significant difference was observed during absorption. The rose was kept in the PEDOT-S solution for about 48 hours. During absorption, fresh 2- to 3-mm cuts to the bottom of the stem were made every 12 hours. After absorption, the bark and phloem were peeled off to reveal the xylem. The dissected stem was kept in DI water under refrigeration until used for characterization and device fabrication.

Xylem wire device fabrication and characterization

The piece of stem was mounted on a Petri dish using UHU patafix and was surrounded by DI water to prevent it from drying out during the experiment. For all the measurements, Au-plated tungsten probe tips (Signatone SE-TG) with a tip diameter of 10 μm were used. Using micromanipulators and viewing under a stereo microscope (Nikon SMZ1500), we brought the probe tips into contact with the wire and applied a very small amount of pressure for the tips to penetrate the xylem and make contact with the PEDOT-S inside.

Xylem wire conductivity measurement

Measurements were performed in the same wire for three different lengths starting from the longest and then placing one contact closer to the other. We used a Keithley 2602B SourceMeter controlled by a custom LabVIEW program. The voltage was swept from 0.5 to −0.5 V with a rate of 50 mV/s.

Xylem-OECT construction

The channel, source, and drain of the OECT are defined by the PEDOT-S wire in the xylem. Contact with source and drain was made using Au-plated tungsten probe tips. A PEDOT:PSS [Clevios PH 1000 with 10% ethylene glycol and 1% 3-(glycidyloxypropyl)trimethoxysilane]–coated probe tip was used as the gate. The tip penetrated the tissue in the vicinity of the channel. All measurements were performed using a Keithley 2602B SourceMeter controlled by a custom LabVIEW program.

NOR gate construction

The NOR gate consisted of two xylem-OECTs and a resistor in series. The two transistors were based on the same PEDOT-S xylem wire and were defined by two gates (PEDOT:PSS–coated Au probe tips), placed in different positions near the PEDOT-S xylem. Using probes, we connected the transistors (xylem wire) to an external 800-kilohm resistor and a supply voltage (V_{DD} = −1.5 V) on one side and grounded them on the other side. All measurements were performed using two Keithley 2600 series SourceMeters that were controlled using a custom LabVIEW program and one Keithley 2400 SourceMeter controlled manually.

Preparation of PEDOT:PSS–NFC material

A previously reported procedure was followed with minor modifications for the preparation of the PEDOT:PSS–NFC material (*28*). Briefly, PEDOT:PSS (Clevios PH 1000, Heraeus) was mixed with dimethyl sulfoxide (Merck Schuchardt OHG), glycerol (Sigma-Aldrich), and cellulose nanofiber (Innventia, aqueous solution at 0.59 wt %) in the following (aqueous) ratio: 0.54:0.030:0.0037:0.42, respectively. The mixture was homogenized (VWR VDI 12 Homogenizer) at a speed setting of 3 for 3 min and degassed for 20 min in a vacuum chamber. To make the dry film electrode, 20 ml of the solution was dried overnight at 50°C in a plastic dish (5 cm in diameter), resulting in a thickness of 90 μm.

Leaf infusion and contact

A leaf was excised from a cut rose stem that was kept in the refrigerator (9°C, 35% relative humidity). The leaf was washed with DI water and blotted dry. The leaf was placed in a syringe containing PEDOT:PSS–NFC and then plunged to remove air. Afterward, the nozzle was sealed with a rubber cap. The plunger was gently pulled (a difference of 10 ml), thereby creating a vacuum in the syringe. The plunger was held for 10 s and then slowly returned to its resting position for an additional 20 s. The process was repeated 10 times. After the 10th repetition, the leaf rested in the solution for 10 min. The leaf was removed, rinsed under running DI water, and gently blotted dry. Infusion was evident by darker green areas on the abaxial side of the leaf surface. As the leaf dried, the color remained dark, indicating a successful infusion of the material. To make contact to the leaf, small drops (1 μl) of the PEDOT:PSS–NFC solution were dispensed on the abaxial side of the leaf. PEDOT:PSS–NFC film electrodes were placed on top of the drops and were air-dried for about 1 h while the leaf remained wrapped in moist cloth.

Electrochromic measurements

Metal electrodes were placed on top of the PEDOT:PSS–NFC film, and optical images (Nikon SMZ1500) were taken every 2 s. A positive voltage potential was applied (Keithley 2400), and the current was recorded by a LabVIEW program every 250 ms for 6 min. The time stamp was correlated with the optical images. The voltage potential was reversed and the process was repeated. Electrochromic effects were observed between ±2 and ±15 V.

Image analysis

The optical images were converted to TIFF (tagged image file format) using the microscope software NIS-Elements BR, opened in ImageJ, and used without further image processing. The grayscale pixel intensity (0 to 255) was recorded for pixels along a straight line (Fig. 6, C and D) by taking the final image (that is, the image after 6 min) for each state: V_1 = +15 V, V_2 = −15 V, and V_3 = +15 V. Each respective image for the three states was sampled 10 times and averaged together. Afterward, those averaged grayscale values were subtracted from the averaged values of the previous state (that is, V_2 from V_1, and V_3 from V_2) representing the changes due to electrochromism plotted in Fig. 6 (E and F). To observe estimated electric field path between the electrodes, the final image of the second run (V_2) was subtracted from the final image of the first run (V_1) in ImageJ to create a false color image of the changes shown in Fig. 7A. Additionally, the final image of the third run (V_3) was subtracted from the second run (V_2). The false color images were increased in brightness and contrast, and noise reduction was applied to reveal the changes in oxidized and reduced states.

SUPPLEMENTARY MATERIALS

Supplementary material for this article is available at http://advances.sciencemag.org/cgi/content/full/1/10/e1501136/DC1

Methods

Fig. S1. PEDOT-infused and electrochromic leaves on living rose.

Table S1. Summary of materials attempted for conducting xylem wires.

Movie S1. Video recording of electrochromism in PEDOT:PSS–NFC–infused rose leaf.

References (*31*–*34*)

REFERENCES AND NOTES

1. P. H. Raven, R. F. Evert, S. E. Eichhorn, *Biology of Plants* (W. H. Freeman, New York, 2005).
2. B. Buchanan, W. Gruissem, R. Jones, *Biochemistry & Molecular Biology of Plants* (Wiley, Hoboken, NJ, ed. 2, 2015).
3. J. M. Leger, Organic electronics: The ions have it. *Adv. Mater.* **20**, 837–841 (2008).
4. X. Wang, B. Shapiro, E. Smela, Visualizing ion currents in conjugated polymers. *Adv. Mater.* **16**, 1605–1609 (2004).
5. A. Jonsson, Z. Song, D. Nilsson, B. A. Meyerson, D. T. Simon, B. Linderoth, M. Berggren, Therapy using implanted organic bioelectronics. *Sci. Adv.* **1**, e1500039 (2015).
6. J. Rivnay, J. Rivnay, P. Leleux, M. Ferro, M. Sessolo, A. Williamson, D. A. Koutsouras, D. Khodagholy, M. Ramuz, X. Strakosas, R. M. Owens, C. Benar, J.-M. Badier, C. Bernard, G. G. Malliaras, High-performance transistors for bioelectronics through tuning of channel thickness. *Sci. Adv.* **1**, e1400251 (2015).
7. L. Ouyang, C. L. Shaw, C. C. Kuo, A. L. Griffin, D. C. Martin, In vivo polymerization of poly(3,4-ethylenedioxythiophene) in the living rat hippocampus does not cause a significant loss of performance in a delayed alternation task. *J. Neural Eng.* **11**, 026005 (2014).
8. M. Hamedi, A. Elfwing, R. Gabrielsson, O. Inganäs, Electronic polymers and DNA self-assembled in nanowire transistors. *Small* **9**, 363–368 (2012).
9. L. Groenendaal, F. Jonas, D. Freitag, H. Pielartzik, J. R. Reynolds, Poly(3,4-ethylenedioxythiophene) and its derivatives: Past, present, and future. *Adv. Mater.* **12**, 481–494 (2000).
10. R. H. Karlsson, A. Herland, M. Hamedi, J. A. Wigenius, R. Åslund, X. Liu, M. Fahlman, O. Inganäs, P. Konradsson, Iron-catalyzed polymerization of alkoxysulfonate-functionalized 3,4-ethylenedioxythiophene gives water-soluble poly(3,4-ethylenedioxythiophene) of high conductivity. *Chem. Mater.* **21**, 1815–1821 (2009).
11. E. Stavrinidou, P. Leleux, H. Rajaona, D. Khodagholy, J. Rivnay, M. Lindau, S. Sanaur, G. G. Malliaras, Direct measurement of ion mobility in a conducting polymer. *Adv. Mater.* **25**, 4488–4493 (2013).
12. D. Nilsson, M. Chen, T. Kugler, T. Remonen, M. Armgarth, M. Berggren, Bi-stable and dynamic current modulation in electrochemical organic transistors. *Adv. Mater.* **14**, 51–54 (2002).
13. J. Bobacka, Potential stability of all-solid-state ion-selective electrodes using conducting polymers as ion-to-electron transducers. *Anal. Chem.* **71**, 4932–4937 (1999).
14. F. Louwet, The organic alternative to ITO. *Dig. Tech. Pap. Soc. Inf. Disp. Int. Symp.* **39**, 663–664 (2008).
15. S. Ghosh, O. Inganäs, Networks of electron-conducting polymer in matrices of ion-conducting polymers. Applications to fast electrodes. *Electrochem. Solid-State Lett.* **3**, 213–215 (2000).
16. B. Winther-Jensen, O. Winther-Jensen, M. Forsyth, D. R. MacFarlane, High rates of oxygen reduction over a vapor phase-polymerized PEDOT electrode. *Science* **321**, 671–674 (2008).
17. P. Andersson, D. Nilsson, P.-O. Svensson, M. Chen, A. Malmström, T. Remonen, T. Kugler, M. Berggren, Active matrix displays based on all-organic electrochemical smart pixels printed on paper. *Adv. Mater.* **14**, 1460–1464 (2002).
18. D. Nilsson, N. Robinson, M. Berggren, R. Forchheimer, Electrochemical logic circuits. *Adv. Mater.* **17**, 353–358 (2005).
19. E. Masarovičová, K. Kráľová, Metal nanoparticles and plants. *Ecol. Chem. Eng. S* **20**, 9–22 (2013).
20. J. P. Giraldo, M. P. Landry, S. M. Faltermeier, T. P. McNicholas, N. M. Iverson, A. A. Boghossian, N. F. Reuel, A. J. Hilmer, F. Sen, J. A. Brew, M. S. Strano, Plant nanobionics approach to augment photosynthesis and biochemical sensing. *Nat. Mater.* **13**, 400–408 (2014).
21. D. Djikanović, A. Kalauzi, M. Jeremić, J. Xu, M. Mićić, J. D. Whyte, R. M. Leblanc, K. Radotić, Interaction of the CdSe quantum dots with plant cell walls. *Colloids Surf. B Biointerfaces* **91**, 41–47 (2012).
22. H. I. Hussain, Z. Yi, J. Rookes, L. X. Kong, D. M. Cahill, Mesoporous silica nanoparticles as a biomolecule delivery vehicle in plants. *J. Nanopart. Res.* **15**, 1676 (2013).
23. P. Kanhed, S. Birla, S. Gaikwad, A. Gade, A. B. Seabra, O. Rubilar, N. Duran, M. Rai, In vitro antifungal efficacy of copper nanoparticles against selected crop pathogenic fungi. *Mater. Lett.* **115**, 13–17 (2014).
24. D. M. Miller, Studies of root function in *Zea mays*: III. Xylem sap composition at maximum root pressure provides evidence of active transport into the xylem and a measurement of the reflection coefficient of the root. *Plant Physiol.* **77**, 162–167 (1985).
25. L. Bernstein, Method for determining solutes in the cell walls of leaves. *Plant Physiol.* **47**, 361–365 (1971).
26. B. M. O'Leary, A. Rico, S. McCraw, H. N. Fones, G. M. Preston, The infiltration-centrifugation technique for extraction of apoplastic fluid from plant leaves using Phaseolus vulgaris as an example. *J. Vis. Exp.* **94**, e52113 (2014).
27. G. Lohaus, K. Pennewiss, B. Sattelmacher, M. Hussmann, K. Hermann Muehling, Is the infiltration-centrifugation technique appropriate for the isolation of apoplastic fluid? A critical evaluation with different plant species. *Physiol. Plant.* **111**, 457–465 (2001).
28. J. Kawahara, P. A. Ersman, X. Wang, G. Gustafsson, H. Granberg, M. Berggren, Reconfigurable sticker label electronics manufactured from nanofibrillated cellulose-based self-adhesive organic electronic materials. *Org. Electron.* **14**, 3061–3069 (2013).
29. S. Ramakrishnan, C. Shannon, Display of solid-state materials using bipolar electrochemistry. *Langmuir* **26**, 4602–4606 (2010).
30. E. Said, N. D. Robinson, D. Nilsson, P.-O. Svensson, M. Berggren, Visualizing the electric field in electrolytes using electrochromism from a conjugated polymer. *Electrochem. Solid-State Lett.* **8**, H12–H16 (2005).
31. K. M. Persson, R. Karlsson, K. Svennersten, S. Löffler, E. W. H. Jager, A. Richter-Dahlfors, P. Konradsson, M. Berggren, Electronic control of cell detachment using a self-doped conducting polymer. *Adv. Mater.* **23**, 4403–4408 (2011).
32. R. Gabrielsson, thesis, Linköping University (2012).
33. T. A. Skotheim, J. Reynolds, *Conjugated Polymers: Theory, Synthesis, Properties, and Characterization* (CRC Press, Boca Raton, FL, 2006).
34. H. E. Gottlieb, V. Kotlyar, A. Nudelman, NMR chemical shifts of common laboratory solvents as trace impurities. *J. Org. Chem.* **62**, 7512–7515 (1997).

Acknowledgments: We thank M. Grebe and D. Poxson for help in initiating the project, R. Forccheimmer for assistance with circuit analysis, A. Malti and J. Edberg for assistance with the NFC material, and D. Khodagholy and I.-A. Apolozan for assistance with the LabVIEW programs. **Funding:** This project was funded primarily by a Knut and Alice Wallenberg Foundation Scholar grant to M.B. (KAW 2012.0302). Additional funding was provided by Linköping University and the Önnesjö Foundation. **Author contributions:** E.S. tested materials for developing conducting xylem wires; performed electrical characterization, optical microscopy, and SEM of the PEDOT-S:H wires; developed the OECT and NOR logic gate; and analyzed all corresponding data. R.G. synthesized and tested materials for developing conducting xylem wires. E.G. and E.S. developed the leaf-OECD. E.G. performed optical microscopy, electrochromic measurements, image analysis, and the in vivo experiment of leaf-OECD, and designed all figure illustrations. M.B., E.G., D.T.S., and E.S. developed the electrical representation of the leaf-OECD. All authors contributed to the initial draft. M.B. and D.T.S. wrote the final manuscript. O.N. was responsible for the plant physiology relevance. M.B., D.T.S., X.C., and O.N. supervised the project. M.B. conceived the project. **Competing interests:** The authors declare that they have no competing interests. **Data and materials availability:** All data needed to evaluate the conclusions in the paper are present in the paper and/or the Supplementary Materials. Additional data related to this paper may be requested from the authors. The data are available upon request to E.S. and E.G., and the materials are available upon request to R.G.

Submitted 21 August 2015
Accepted 7 October 2015
Published 20 November 2015
10.1126/sciadv.1501136

Citation: E. Stavrinidou, R. Gabrielsson, E. Gomez, X. Crispin, O. Nilsson, D. T. Simon, M. Berggren, Electronic plants. *Sci. Adv.* **1**, e1501136 (2015).